Optimization of Triple Periodic Bilayer Stacks and Aerial Image Performance Analysis

Zhen Zhang
School of Information Science and Engineering, Shandong University (Qingdao), Binhai Road 72, 266237, Qingdao, China
Email: 411632071@qq.com

***Abstract*—EUV lithography uses 13.5 nm wavelength incident light. For all materials, the absorption of EUV wavelength cannot be neglected. Therefore, EUV lithography system employs a reflective system. In order to to increase the reflectivity rate, We optimize triple periodic bilayer stacks for 13.5 nm EUV- lithography with a 4 × demagnification and an Numerical Aperture (NA) of 0.5. The optimization is performed using multi-objective Genetic Algorithms (GA). Selected bilayer stacks are further investigated by adding a 9.5 nm dense line absorber. The aerial images are calculated and the lithographic performance of these mask designs are evaluated in terms of threshold, NILS, EL and DOF.**

***Index Terms*—optimization, bilayer stacks, aerial image**

I. Introduction

Extreme Ultraviolet lithography (EUV) is the next generation technology using 13.5 nm wavelength incident light. In the year of 2011, ASML launched a pre-production named NXE: 3100 with an NA of 0.25, which offered a resolution of 27 nm and showed stable performance [1]. In 2013, NXE: 3300B platform with an NA of 0.33, achieved a resolution of 22 nm and beyond [2]-[4].

EUV lithography employs reflective system because for all materials, the absorption of EUV wavelength cannot be neglected. Therefore, the mask has to be exposed to oblique incidence to separate the incident and reflected light. For EUV system employing numerical aperture 0.5 and a demagnification of M =4, the Chief Ray Angle at Object side (CRAO) is set to be 9° [5]. The incident bundle of light is in an angle range of $9° \pm \arcsin(0.5 / 4)$, namely $1.8° \sim 16.3°$. This requires the lithographic reticle designed to reflect the light over the abovementioned range of incident angles.

A EUV mask usually consists of two parts, an absorber material to form the pattern, and a dielectric mirror, to increase the reflectivity of the incident light [6], [7]. The dielectric mirror part consists of 40 or more bilayers of materials with alternating higher and lower refractive index, more specific, Mo and Si [7]. The thickness of Mo and Si layers is optimized to provide a high reflectivity over a certain range of incidence angles. Single and double bilayer stacks cannot provide sufficient reflectivity over the range of incident angles for high NA EUV imaging system, therefore, in this paper, we choose to optimize triple bilayers which consist of upper, middle and lower sections (see Fig. 1), which results in 9 optimization variables: thickness of Mo and Si in upper, middle, and lower sections, and number of bilayers in each section.

The optimization is performed by a multi-objective genetic algorithm [8], [9], which is integrated in Dr. LiTHO, a software developed by Fraunhofer IISB, Erlangen, Germany. A pareto front is generated [10], [11] and three designs are selected for further investigation.

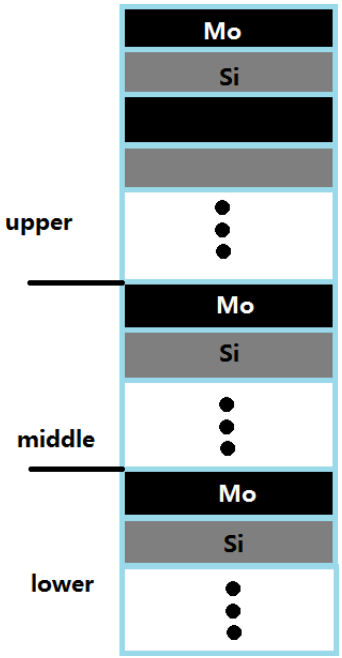

Figure 1. Schematic presentation of three periodic MoSi bilayer-stacks.

II. Optimization of MoSi Bilyaer Stakcs

The goal of the optimization has two aspects, to maximize the average reflectivity rate ⟨R⟩, and to minimize the Standard Deviation (SD) of the reflectivity rate, which means to maximize the reciprocal of SD. The average reflectivity rate ⟨R⟩ and SD are defined as follows:

Manuscript received May 22, 2020; revised August 12, 2020.

doi: 10.18178/ijeee.8.3.53-57

$$\langle R\rangle = \frac{1}{\theta_{max}-\theta_{min}}\int_{\theta_{min}}^{\theta_{max}}\big(R(\theta)\big)\,d \quad (1)$$

$$SD = \sqrt{\frac{1}{N}\sum_{1}^{N}(R(\theta)-\langle R\rangle)} \quad (2)$$

For this conflicting goal, no single solution exists that simultaneously fulfill the two aspects. Therefore, we use the multi-objective GA to generate a set of solutions, which do NOT dominate each other [12]. As one can see in Fig. 2, Design A shows high reflectivity rate, Design C exhibits relatively flat curve, while the performance of Design B falls in the middle between A and C. Fig. 3 shows the calculated reflectivity rate of the three designs versus the incident angle range.

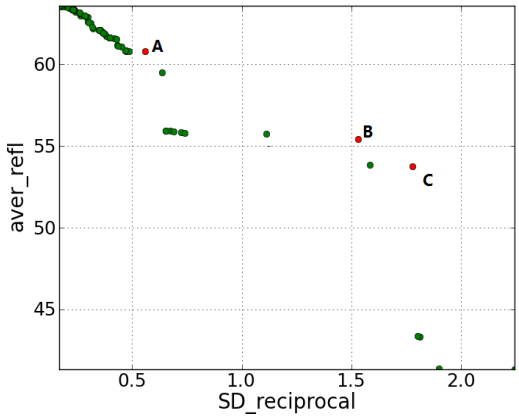

Figure 2. The Pareto front for multi- objective optimization of MoSi 3-period stacks.

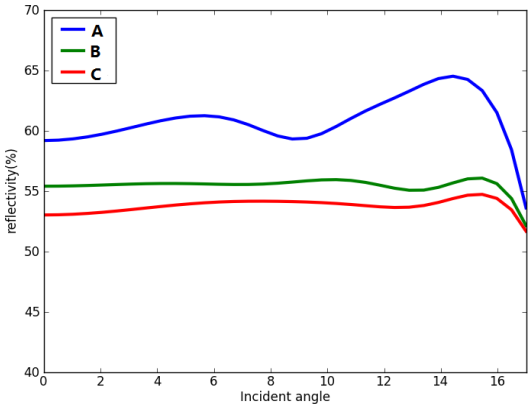

Figure 3. Computed reflectivity rate of Design A, B, C versus incident angle range.

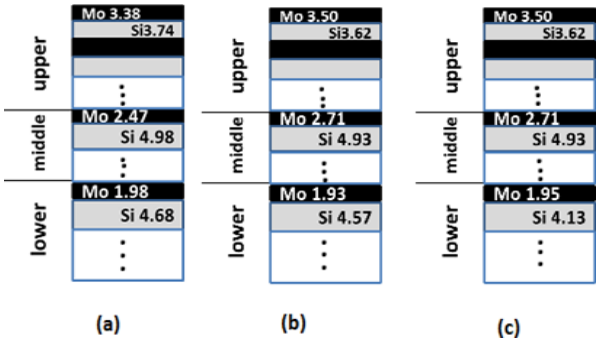

Figure 4. Parameter settings of the selected optimized stacks, from left to right, Design A, B, and C, respectively.

Design A consists of 20 upper, 17 middle and 19 lower bilayers. Design B consists of 17 upper, 12 middle, and 14 lower bilayers. Design C consists of 16 upper, 12 middle, and 15 lower bilayers. The thickness distributions of Mo and Si in each bilayer are shown in Fig. 4.

III. Computed Aerial Images

In this section, the absorber feature is added onto the multi-layer stack Design A, B, and C and the resulted aerial images are computed respectively. The required oblique illumination of EUV masks introduces an orientation dependence of the diffraction and imaging characteristics. The illumination is tilted in the XZ-plane by an angle θ to the z-axis. Horizontal Y-parallel lines experience an asymmetric shadowing effect. The left side of the absorber in negative X-direction sees less light than the right side of the absorber in positive X-direction. Vertical X-parallel lines see the same amount of light on both sides of the absorber. Fig. 5 is a schematic diagram of X, and Y parallel feature masks. Due to the oblique incidence and the fact that the dimension of absorber is relatively large compared to the incident wavelength, Y-parallel lines experience shadowing effect [2], [13]. In below we analyze the performance of both Y and X parallel feature masks, respectively.

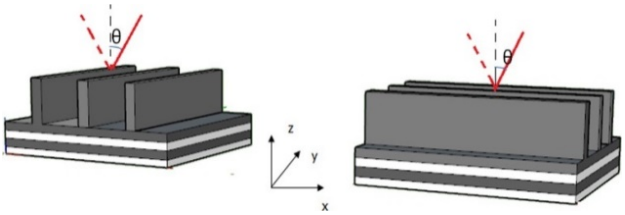

Figure 5. Schematic representation of Y (left) and X (right) parallel lines on an EUV stack.

A. Y-parallel Feature

We add the Y-parallel lines onto the multi-layer stack Design A. Fig. 6 shows a 9.5 nm Y parallel dense line feature. The mask is assumed periodic outside the shown area.

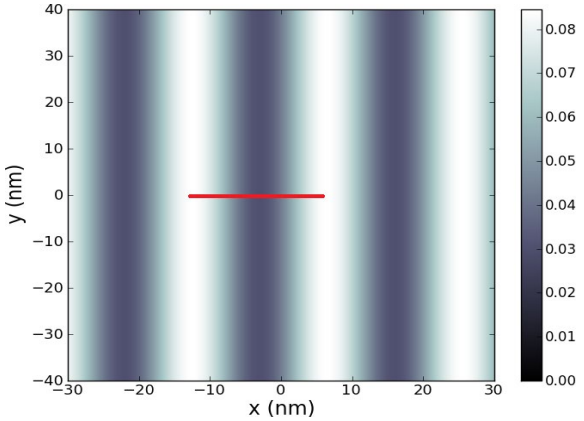

Figure 6. Mask layout plotting of a 9.5 dense line feature.

The blue box indicates the area where the aerial image is computed and plotted. Fig. 7 shows the computed

aerial image with stack A, the red line indicates the cutline which is extracted and further examined in terms of Process window, NILS, and other lithographic criteria.

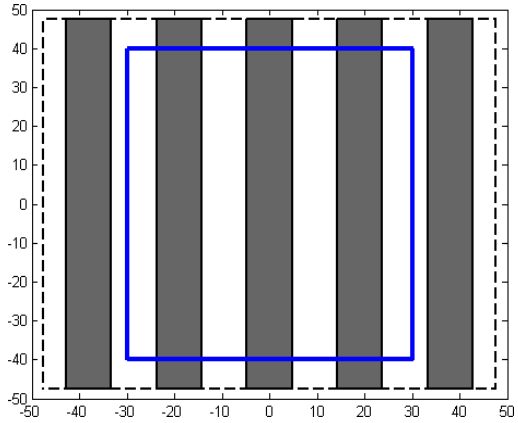

Figure 7. Aerial image computed from the dense line feature with stack A.

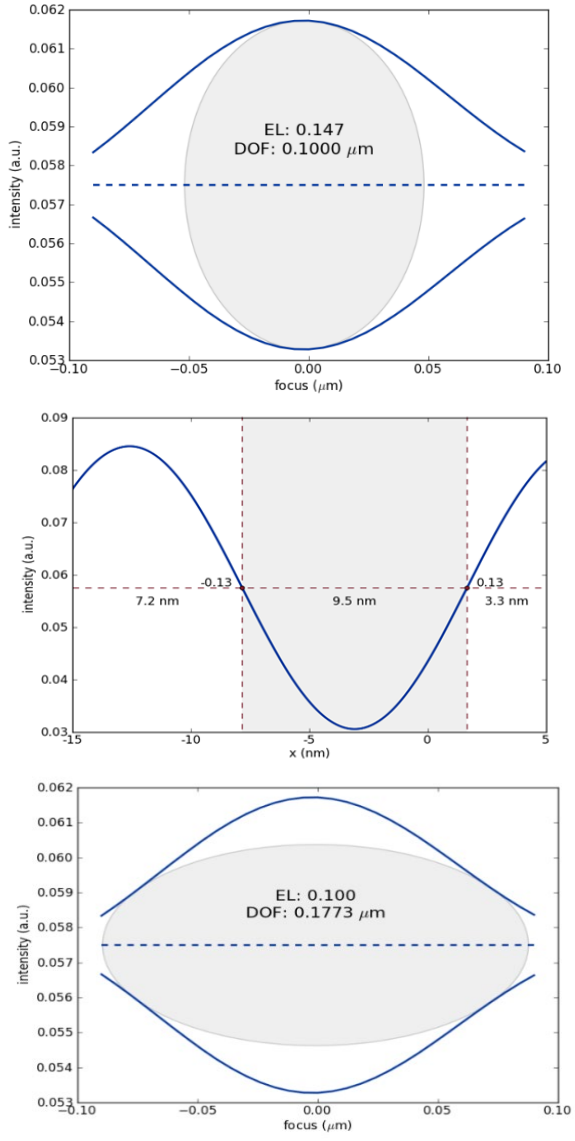

Figure 8. Metrology plot of lithography mask with MoSi stack design A.

Fig. 8a shows the cross section of the extracted cutline. A cross section is a plot of intensity distribution along a line in the image plane, in this case, the red line in Fig. 7. From Fig. 7 and Fig. 8a one can see that the asymmetric shadowing effect not only affects the aerial image, but also the cross section. Threshold to size and NILS are also calculated from Fig. 8a.

Threshold is defined as following:

$$thr = \frac{a}{d-b} \tag{3}$$

where a and b are process-related empirical constants, which depend on the processing conditions and d denotes exposure dose [14]. A higher threshold results in lower dose value, which means shortening exposure time and high efficiency.

NILS characterizes the steepness of the intensity distribution near the nominal edge of the feature, which is defined as following:

$$NILS = \omega \frac{d(lnI(x))}{dx} \tag{4}$$

where $I(x)$ is the intensity, x is the spatial coordinate of the cross section, w is the linewidth of the target feature, in this case, 9.5 nm dark feature, or so called Critical Dimension (CD). A large NILS means a strong contrast of bright and dark feature. The threshold and NILS of Design A is listed in Table 1.

Fig. 8b and Fig. 8c shows the process window for a given DOF and a given Exposure Latitude (EL) respectively [15]. EL denotes exposure latitude, which is determined by ratio of the maximum dose error range and threshold.

Depth of Focus (DOF) is defined as following:

$$DOF = k_2 \frac{\lambda}{NA^2} \tag{5}$$

where the parameter k_2 is second technology factor, which depends from the features to be imaged, illumination geometry, photoresist, processing conditions and other details. NA is numerical aperture on the wafer side. Large DOF means large range of focus errors that a process can tolerate. The DOF is usually specified for the smallest features to be imaged. The diffraction spectrum of larger features is focused around the center of the projection pupil. The resulting optical path differences and defocus effects are less pronounced for such large features.

Process window represents CD versus dose and defocus dependency. In Fig. 8b, the upper curve shows the dose values to generate features with 90% of target CD, while the lower curve shows the dose values to generate features with 110% of target CD. All combinatins of dose and defocus between the upper and lower curve produce the target with an accuracy of $\pm$ 10 %. As one can see in Fig. 8b, an ellipse fitted into the process window shows that for a giving DOF, the biggest EL is 0.147.

Similarly, we calculate the aerial images for Design B, and C, and extract all the evaluated parameters from the same cutline. All parameters are summarized in Table I.

TABLE I. METROLOGY PARAMETERS FOR Y-PARALLEL DENSE LINE FEATURE COMBINED WITH MOSI BILAYER DESIGN A, B AND C

Design	⟨ R ⟩	SD	Threshold	NILS	EL	DOF [μm]
A	60.8%	1.79	0.057	1.244	0.147	0.1773
B	55.4%	0.65	0.044	0.980	0.115	0.1530
C	53.87%	0.56	0.041	0.890	0.105	0.1370

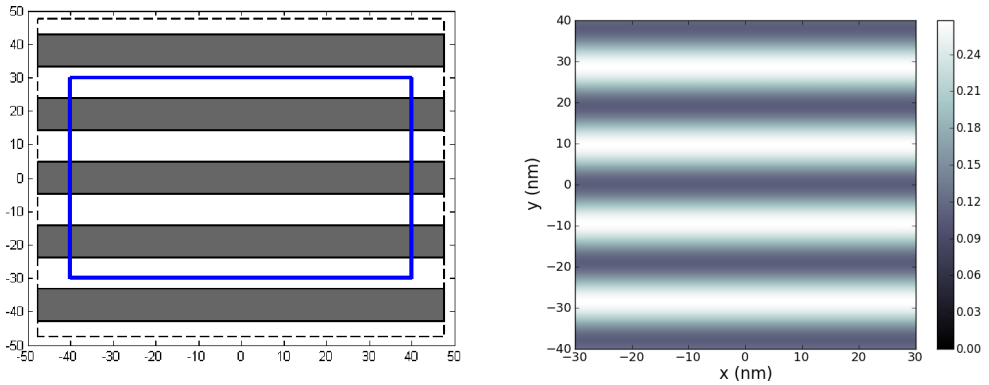

Figure 9. Left: the mask layout of x- parallel dense line feature, linewidth as 9.5 nm in wafer size. Right: the aerial image of Design A.

TABLE II. METROLOGY PARAMETERS FOR X-PARALLEL DENSE LINE FEATURE COMBINED WITH MOSI BILAYER DESIGN A, B AND C

Design	⟨ R ⟩	SD	Threshold	NILS	EL	DOF [μm]
A	60.8%	1.79	0.209	1.093	0.129	0.1662
B	55.4%	0.65	0.190	1.122	0.132	0.1687
C	53.87%	0.56	0.184	1.132	0.133	0.1695

B. X-parallel Feature

From Fig. 9 one can see that the X-parallel feature does not experience shadowing effect. Similarly, the aerial images of Design B, and C are computed, and all evaluated parameters are summarized in Table II.

IV. CONCLUSIONS

From Table I and Table II one can see that:

1) High average reflectivity results in high threshold. The largest threshold (the highlighted item) is obtained from Design A.

2) For Y-parallel dense line feature, Design A, which exhibits the biggest reflectivity rate, has the largest NILS and DOF range.

3) For X-parallel feature, Design C, which exhibits the smallest SD, has the largest NILS and DOF range.

4) For X, and Y-parallel feature, the NILSs and DOFs are different, in general, the NILS and DOF of Y-parallel feature are smaller (expect for Design A). Shadowing effect plays a role in generating such a difference: for imaging close to the resolution limit, only two diffraction orders (0th, 1st.) contribute to the image formation. The contrast of the resulting interference pattern is determined by the intensities of these orders. It has been computed by Neumann *et al.*, that due to shadowing effect -1st. diffraction order is much weaker than 0.th order, the intensity imbalance between the two orders would further results in lower interference contrast. Second, the above values are computed on the focal plane, while the large thickness of absorber leads to best focus shift.

CONFLICT OF INTEREST

The author declare no conflict of interest.

REFERENCES

[1] R. Peeters, "EUV lithography NXE platform performance overview," presented at the SPIE Advanced Lithography, San Jose CA, 2014, pp. 9048-9054.

[2] J. Neumann, P. Graeupner, W. Kaiser, R. Garreis, and B. Geh, "Mask effects for high-NA EUV: Impact of NA, chief-ray-angle, and reduction ratio," in *Proc. SPIE*, 2013, vol. 8679, p. 867915.

[3] R. Peters, "ASML's NXE platform performance and volume introduction," in *Proc. SPIE*, 2013, vol. 8679, p. 867950.

[4] M. Lowisch, "Optics for ASML's NXE: 3300 platform," in *Proc. SPIE*, 2013, vol. 8679, p. 867952.

[5] A. Erdmann, "Modeling studies in alternative EUV mask comcepts for higher NA," in *Proc. SPIE*, 2013, vol. 8679, p. 86791Q.

[6] J. Ruoff, "Impact of mask topography and multilayer stack on high NA imaging of EUV masks," in *Proc. SPIE*, 2010, vol. 7823, p. 78231N.

[7] M. Singh and J. Braat, "Design of multilayer extreme-ultravoilet mirrors for enhanced reflectivity," *Applied Optics*, vol. 39, no. 13, pp. 2189-2197, 2000.

[8] T. Fuehner, A. Erdmann, and S. Seifert, "Direct optimization approach for lithographic process conditions," *Journal of Micro/Nanolithography, MEMS, and MOEMS*, vol. 6, no. 3, p. 031006, 2007.

[9] T. Fuehner, P. Evanschitzky, and A. Erdmann, "Mutual source, mask and projector pupil optimization," *Proc. of SPIE*, 2012, vol. 8322, p. 83220I.

[10] K. Deb, *Multi-Objective Optimization Using Evolutionary Algorithms*, New York: John Wiley & Sons, 2001.

[11] L. Wang, *Multi-objective Evolutionary Optimisation for Product Design and Manufacturing*, London: Springer, 2011.
[12] Wiki. Multi-objective Optimization. [Online]. Available: https://en.wikipedia.org/wiki/Multi-objective_optimization
[13] P. Yan, "EUV mask absorber characterization and selection," in *Proc. of SPIE*, 2000, vol. 4066, pp.115-123.
[14] D. Fuard, "Assessment of different simplified resist models," in *Proc. of SPIE*, 2002, vol. 4691, pp.1266-1277.
[15] R. Voelkel, "Lithographic process window optimization for mask aligner proximity lithography," presented at the SPIE Advanced Lithography, 2014, p. 9052-15.

Zhen Zhang got her bachelor degree at Shandong University in 2006, majoring Optical information Science and Engineering. She got a master degree in 2009, also at Shandong University, majoring Optical Engineering. In 2015, she got a second master degree at Erlangen University, Germany, majoring advanced optical technologies. She works as an assistant Engineer since 2016 at Shandong University.